Part I
Survey

Bernhard Kramer
I. Institut für Theoretische Physik
Universität Hamburg
Jungiusstraße 9
20355 Hamburg
Germany

1 Survey of mesoscopic quantum transport

Semiconductor inversion layers provide an outstanding laboratory for the investigation of quantum mechanical phenomena in condensed matter, since many of their properties like charge carrier density and mobility can be adjusted by external means.

During the past two decades, a great variety of quantization and coherence effects in their electrical transport properties have been discovered. The most prominent example is the quantum Hall effect. The finding of the quantization of the Hall conductivity of MOSFETs in integer multiples of e^2/h at low temperatures and sufficiently strong magnetic fields initiated a veritable "industry" of experimental and theoretical research. The *integer quantum Hall effect* (IQHE) established a completely new tool for the investigation of localization phenomena since the dynamics of the electrons in the inversion layer of a MOSFET are subject to the random distribution of impurities. The subsequent discovery of the *fractional quantum Hall effect* (FQHE) gave rise to totally unexpected developments concerning the effects of the Coulomb interaction. Novel phases of the interacting two dimensional electronic system, like the "incompressible electron fluid", were found. New routes to well known concepts like the Wigner crystal suddenly became experimentally accessible.

With refined preparation techniques, it became possible to prepare inversion layers that are laterally structured on a nanometer scale. Quasi one dimensional (1D) inversion layers exhibit unique quantization and fluctuation phenomena. Systems of two dimensional point contacts were designed to form islands of electrons, quantum dots, which showed characteristic oscillatory transport behaviour — the signature of the Coulomb repulsion between the electrons. Arrays of quantum dots were found to permit the systematic experimental study of the signatures of chaos in quantum systems. The theoretical prediction of persistent currents in normally conducting metals was experimentally verified by using a structured inversion layer embedded in an AlGaAs/GaAs heterostructure. The field is still rapidly developing.

In the following, a brief survey of the mesoscopic quantum transport effects in nano-structured "metallic" samples discovered during the past two decades is given, in order to provide the background for the effects to be discussed in this Landolt-Börnstein volume. Furthermore to provide a complete panorama of the effects, non-semiconductor based systems are also included.

1.1 Summary of semi-classical description of electrical transport

In this Section, the elements of the semi-classical description of electrical transport are briefly summarized as the background for the effects to be described below. Characteristic length scales are introduced which have turned out to be extremely useful when discussing the conditions for "mesoscopic transport behaviour" of a sample.

1.1.1 Semi-classical electron transport

The electrical current I through a metallic solid is due to the motion of electrons as a consequence of an applied voltage U. The physical origin of the *electrical resistance* of a metal

$$R = \frac{U}{I} \tag{1}$$

is related to the scattering of the electrons due to imperfections in the lattice of the atoms [72Z, 76A]. At higher temperatures, irregular thermal motion of the lattice atoms predominantly influences the electron motion. At temperatures near absolute zero thermal vibrations of the lattice are frozen out. Impurities, defects, dislocations and other static perturbations are then the only obstacles to the electronic motion. The corresponding scattering processes in this region are the only limiting processes for electron transport. Thus, the electrical resistance R is here practically independent of the temperature T. The resistance at $T = 0$ is called the *residual resistance*, or *Restwiderstand*. On the other hand, the scattering of the electrons by the lattice vibrations, the *phonons*, depends on temperature. They dominate at room temperature, where one observes

$$R \propto T\,. \tag{2}$$

The resistance of a piece of metal depends not only on its microscopic properties but also on its geometrical shape and size. In the conventional theory of metallic resistance it is assumed that one can decompose

$$R = \rho(T\ldots) f(\text{geometry}) \tag{3}$$

where the *resistivity* ρ contains the microscopic information about the sample, and f depends on its geometrical shape and size. For instance, for a rectangular bar of length L and cross-sectional area A, $f = L/A$; the resistance of a d-dimensional hypercube is similarly

$$R = \rho L^{(2-d)}\,. \tag{4}$$

Examples for the typical low-temperature behaviour of the resistance are shown in Fig. 1 [50M].

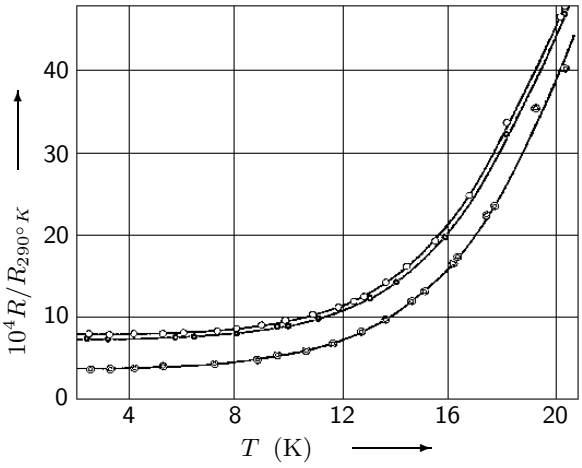

Fig. 1: The electrical resistance R of sodium below 20 K for three different specimens [50M] as a function of the temperature T.

The inverses of electrical resistance and resistivity are the *electrical conductance* $S = R^{-1}$ and the *electrical conductivity* $\sigma = \rho^{-1}$, respectively. The conductivity connects the driving electric field E with the current density j,

$$j = \sigma E\,. \tag{5}$$

For non-isotropic systems, in which the directions of current and driving fields do not necessarily coincide, resistance (resistivity) and conductance (conductivity) are tensors and are then related

by matrix inversion. In non-homogeneous systems, the above relation between current density and electric field is non-local.

In a metallic system, due to the periodic potential of the atom cores, the electronic states are characterized by an *effective mass* m^* which is in general different from the bare electron mass m_0. The larger m^* the smaller is the velocity which an electron can gain within a given period of time when accelerated by a driving electric field. The mean electron velocity increases with the length of the time interval, τ. Furthermore, the current density is also proportional to the number density of the electrons n yielding

$$\sigma = \frac{ne^2\tau}{m} . \tag{6}$$

This classical theory of electrical transport was developed around the turn of the 19th century by Paul Drude (1863-1906). The time interval τ is the *mean free time* between two scattering processes, which the electron suffers during its diffusive motion under the influence of the driving field. A microscopic theory of transport is therefore necessarily a theory of the *scattering time* τ. It has been noted only in the latter part of the 20th century, in connection with the discovery of the mesoscopic transport phenomena, that there are two essentially and conceptually different kinds of scattering processes in metallic and semiconducting samples. *Coherent* scattering (*elastic mean free time* τ) does not destroy the quantum mechanical phase of the electron, while *phase-breaking* scattering (*phase breaking time* τ_ϕ) does. The former is usually associated with *impurity scattering*, while the latter is related to the interactions between the electrons as well as between electrons and other degrees of freedom in the system, such as lattice vibrations. The distinction between the different kinds of scattering processes is very important at low temperatures. Here, there is yet another characteristic time which becomes relevant, the *temperature-induced decoherence time* $\tau_T \propto (k_B T)^{-1}$. It is due to averaging over the energy interval $k_B T$.

If several scattering mechanisms contribute to the electrical resistance, the corresponding scattering rates τ_i^{-1} have to be added,

$$\tau^{-1} = \sum_i \tau_i^{-1} . \tag{7}$$

This is *Matthiesens's rule* of semi-classical transport in metals.

At very low temperatures, the phase breaking processes, which are induced by interactions, are "frozen out". The electrons are practically only scattered by the impurities and the low-temperature resistance is expected to become independent of T (Restwiderstand). However, for $T \to 0$ the quantum mechanical nature of the electrons has to be taken into account. The coherence of the electronic wave functions, which can extend throughout the whole crystal, cannot be neglected. It turns out that quantum effects can enhance the impurity scattering so strongly that the low-temperature resistance of "classically" normal-metallic systems can diverge at $T = 0$.

The quantum mechanical theory of transport is a subject of considerable current research. While there has been some recent progress for non-interacting particles, the transport theory for interacting particles in disordered systems is, even near the transition from metallic to insulating behaviour, still in its infancy.

1.1.2 Characteristic length scales

In this Section, we introduce the characteristic length scales which correspond to the above characteristic times.

The *mean free path* ℓ is defined by

$$\ell = v_F \tau . \tag{8}$$

It is the distance which an electron with Fermi velocity v_F travels within the mean free time τ. The scattering rate is proportional to the number density of the impurities and the strength of their potential. The latter is usually described by a parameter characterizing the "disorder" in the

metal, W^2. Therefore,

$$\ell \propto \frac{1}{W^2}\,. \tag{9}$$

Measuring the resistance near $T = 0$ provides a measure of the disorder in the sample.

At low temperatures, the electrons move diffusively under the influence of the impurities. Since the phase breaking time is much larger than the mean free time, many elastic scatterings at impurities occur between two phase breaking processes. The temperature dependent *phase breaking length* $L_\phi(T)$ is defined as

$$L_\phi(T) = \sqrt{D\tau_\phi} \tag{10}$$

where D is the diffusion constant near $T = 0$ which can be deduced from the conductivity via the Einstein relation

$$D = \frac{\sigma}{e^2 n}\,. \tag{11}$$

The temperature dependence of the phase breaking time depends on both the nature of the scattering process and on the system dimensionality. Typically

$$\tau_\phi(T) \propto \frac{1}{T^p} \tag{12}$$

with $p = 1 \ldots 5$.

Similarly, a temperature-induced dephasing length $L_T(T)$ can be defined as

$$L_T(T) = \sqrt{D\tau_T}\,. \tag{13}$$

As long as $p > 1$, the phase breaking time will be determined at low temperatures ($\tau_\phi(T) > \tau_T$), only by the temperature-induced de-phasing, and should diverge for $T = 0$ as $L_T \propto T^{-1/2}$. This is, however, experimentally *not* confirmed [97M]. Presently it seems, according to all available experimental data, that below $T \approx 1\,\mathrm{K}$ the phase breaking time saturates (typically $\tau_\phi \approx 1\,\mathrm{ns}$). Why this should be the case is theoretically not understood.

1.1.3 Conditions for mesoscopic behaviour

The low-temperature phase coherence length $L_\phi(1\,\mathrm{K})$ is typically $\sim 1\,\mu\mathrm{m}$, while for room temperature the mean distance between scattering is of the order of a few nm. In order to observe quantum coherent behaviour of the electrons, it is necessary to reduce the temperature and the size of the samples. Quantum coherence becomes effective in mesoscopic samples as soon as

$$L \approx L_\phi\,. \tag{14}$$

Therefore, typical spatial dimensions of quantum coherent samples are of the order of a few μm. Since the spatial dimensions of these samples are intermediate between atoms and ordinary macroscopic bodies, they are often denoted as *mesoscopic quantum systems*. The transport effects observed in these systems are called *mesoscopic quantum transport phenomena*.

In contrast to ordinary metals, semiconductors have several properties which make them particularly useful for the study of mesoscopic quantum transport. They can be intensionally doped with impurities. Thus, the disorder can be experimentally very precisely controlled. Almost ideal 2D electron layers near interfaces in Silicon MOSFETs or AlGaAs/GaAs heterostructures can be fabricated. The mobility of the electrons in these layers can be very high, up to several $10^6\,\mathrm{Vs/cm^2}$. The mean free path can be as large as $10\,\mu$m, and the electrons can move ballistically over macroscopic distances. Correspondingly, the phase breaking length can also become very large. By applying an external magnetic field, these lengths can be further increased. In summary, semiconductor-based mesoscopic samples provide outstanding systems for the study of mesoscopic quantum physics, in particular in connection with the modern sub-micron structuring techniques of the semiconductor device industry, as, for instance, electron-beam lithography (EBL).

1.2 Summary of low temperature quantum transport

The low temperature quantum transport effects discovered in the past years are summarized in the table below. Some of the phenomena have been discovered in metallic and even superconducting samples. They are nevertheless intrinsically independent of the material. Therefore, in this introductory chapter, we do not distinguish between materials, for the sake of a broad overview.

Table 1: The low temperature quantum transport effects.

year	effect	description	reference
1979	weak localization	quantum correction to low temperature conductivity of metals; logarithmic increase of resistance with decreasing temperature; negative magnetoresistance	[79G] [79A] [79D] [84B]
1980	integer quantum Hall effect	quantization of Hall conductivity of a MOSFET in units of e^2/h at integer filling factors; vanishing of the magneto-conductance near these fillings	[80K] [86vK]
1981	AB-oscillations	quantum interference oscillations of the magnetoresistance of normal metallic cylinders and rings; in cylinders periodicity $2\Phi_0$, in rings Φ_0	[81A] [81S]
1982	conductance fluctuations	non-periodic, static, reproducible fluctuations of the conductance of small metallic electron systems induced by coherent impurity scattering	[82F] [84U]
1982	fractional quantum Hall effect	quantization of Hall conductivity of MOSFET at fractional filling factors; minima of the magneto-conductance near these fillings	[82T]
1988	quantization of conductance in point contacts	quantization of the conductance of constrictions of the electrons in two dimensional electron gases in semiconductor heterostructures	[88W] [88vW]
1990	conductance oscillations in quantum dots	periodic oscillations of the conductance of quantum dots	[89F] [90M]
1990	persistent currents	persistent currents in normal-metallic rings induced into the ground state by an Aharonov-Bohm flux piercing the ring	[90L] [91C] [93M]

1.3 Description of the experimental observations

1.3.1 Quantum corrections to metallic conductivity

It has been only in the late 70ies, that quantum corrections to the normal-metallic conductivity have been discovered in experiments, after early theoretical work which noticed that the perturbation expansion for the conductivity could be summed [66L]. An important consequence of the combined experimental and theoretical efforts has been the discovery that impurity scattering is conceptually completely different from scattering resulting from interactions. The latter destroys the quantum mechanical coherence of the electron states, while the former is *coherent*.

1.3.1.1 Weak localization

The disorder-induced lowest order correction to the low-temperature conductivity of metallic systems has been discovered theoretically in 1979 [79A, 79G]. It can be represented in the language of Feynman diagrams by so-called maximally crossed diagrams. These represent a "vertex correction" to the semi-classical Drude conductivity which can be represented in this language by so-called ladder diagrams.

The maximally crossed diagrams describe physically electron-(time-reversed)hole pairs which propagate randomly but coherently around closed paths [84B, 84A]. As a time-reversed hole is equivalent to a non-time reversed electron, this is called "Cooperon contribution" to the resistivity. These processes enhance the probability for quantum coherent back-scattering in a dirty metal such that the resistivity increases when—with decreasing temperature—the conditions for coherence improve and the coherence lengths grows. In metallic films in which superconductivity is suppressed down to very low temperatures (for instance AuPd, Cu, Mg) with thicknesses of the order of or less than 10 nm and for temperatures below a few Kelvin, a characteristic logarithmic decrease of the conductance is observed experimentally (Fig. 2) [79D, 81V, 84B],

$$\sigma(T) = \sigma_0 - \frac{2e^2}{h} \log\left(\frac{\tau_\phi}{\tau}\right), \tag{15}$$

which has been attributed to these processes. Here, σ_0 is the semi-classical conductivity which can be obtained by using the mean free path approximation, formally by summing the above ladder diagrams. By applying a magnetic field, the coherent back-scattering can be reduced since the relative phases between time-reversed and non-time reversed paths can be tuned by the magnetic field. Thus, the magneto-resistance is *negative* in this temperature region of "weak localization". This negative magneto-resistance is generally accepted as a signature of weak localization in 2D, in contrast to the positive magneto-resistance which accompanies an interaction-induced logarithmic increase of the low-temperature resistance of metallic systems in the quantum region (see below).

The theory of weak localization has been verified experimentally not only in metallic, but also in semiconductor-based electron systems with high accuracy. Not only can it be used for quantitative determinations of the phase coherence time [84B], which is very important for detecting the dominant scattering processes near the absolute zero, but it is also one of the corner stones of the so-called one-parameter scaling theory of localization. The latter is the presently accepted theory to describe the disorder-induced metal-insulator transition (MIT), which is also often denoted as the Anderson transition (AT) [74T, 85L1, 92V, 93K].

1.3.1.2 Electron-electron interaction

Also the interaction between the electrons leads to characteristic corrections to the low temperature behaviour of the resistance [84A, 84F]. They can be distinguished from weak-localization effects by magnetoresistance measurements, since in the case of interactions a positive magnetoresistance is observed.

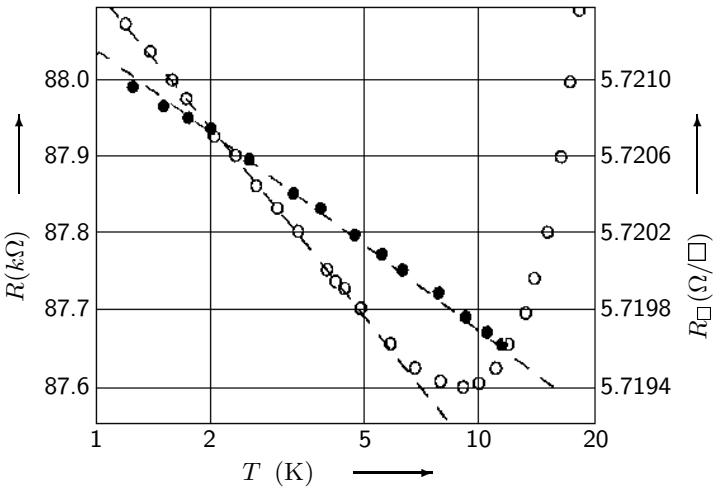

Fig. 2: Logarithmic increase of the resistance of thin metallic films (• metal1 [79D], ∘ metal2 [81V]) at low temperature induced by coherent back scattering from impurities.

1.3.2 Aharonov-Bohm oscillations of magneto-resistance

Direct experimental evidence for the quantum interference suggested by the theory of weak localization to be the backbone of the quantum suppression of transport has been provided by the discovery of Aharonov-Bohm (AB) like oscillations the magneto-conductance of metallic cylinders and rings.

1.3.2.1 Mesoscopic metallic cylinders

The phenomenon of AB-oscillations, resulting from weak-localization corrections, of the magneto-conductance of small metallic cylinders has been predicted by theory [81A], and almost simultaneously verified by experiment in 1981 [81S]. The cylinders were fabricated by evaporating Mg onto quartz filaments. They had diameters of about 1 to 2 μm and lengths of roughly 1 cm. At temperatures of about 1 K, electron states are then coherent around the entire circumference of the cylinders such that they can interfere.

By applying a magnetic field with a direction parallel to the axis of the cylinder, one can generate a well-defined phase shift between electrons which travel clockwise and anti-clockwise around the cylinder,

$$\Delta\varphi(B) = \frac{4\pi e}{h} \oint \boldsymbol{A} \cdot \mathrm{d}\boldsymbol{s} = 2\pi \frac{2\Phi}{\Phi_0}. \tag{16}$$

This phase shift is given by the flux enclosed by the electron paths around the cylinder. When tuning the magnetic flux, the phase shift changes sign for a flux difference of $\Phi_0 = h/e$, the flux quantum. The interference changes from constructive to destructive and *vice versa*. The corresponding oscillations of the magneto-resistance (Figs. 3 and 4) have a periodicity in the magnetic flux of exactly

$$\Delta\Phi = \frac{h}{2e}. \tag{17}$$

The theory of such AB-oscillations is based on the perturbation expansion of the weak localization formalism. It predicts successfully not only the correct periodicity, but also the dependence of the amplitudes of the oscillations as a function of the disorder (mean free time τ) and the frequency of the phase breaking processes (phase coherence time τ_ϕ). From the above measurements, the phase breaking length has been estimated to be about 1 μm in these samples near 1 K.

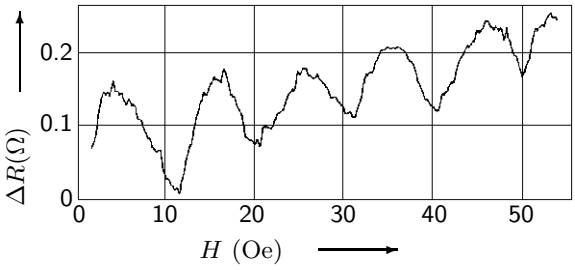

Fig. 3: AB-oscillations in the magneto-resistance of normal metallic Mg cylinders as a function of the magnetic field H at temperature $T = 1.12\,\mathrm{K}$ [81S] and for $R(297\,\mathrm{K})$=12.8 kΩ ($R(4.2\,\mathrm{K})$=9.2 kΩ), diameter 1.58 μm.

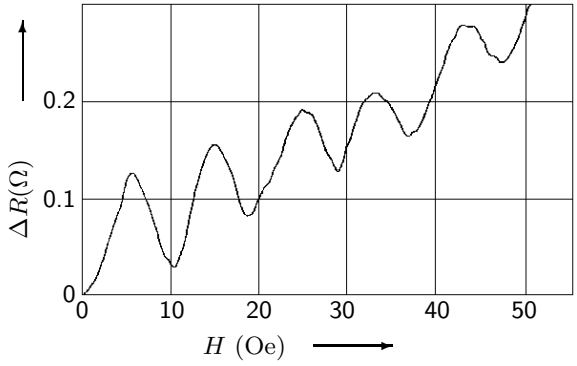

Fig. 4: AB-oscillations in the magneto-resistance of normal metallic Mg cylinders as a function of the magnetic field H at temperature $T = 1.12\,\mathrm{K}$ [81S] and for $R(297\,\mathrm{K})$=15.3 kΩ ($R(4.2\,\mathrm{K})$=12.3 kΩ), diameter 1.58 μm.

1.3.2.2 Networks of rings

The above magneto-resistance oscillations, characterized by the periodicity $\Phi_0/2$ (17) have been found to exist also in networks of rings made of normal metallic materials [84P]. Using a Mg-network consisting of about 2.7×10^6 identical hexagonal loops forming a regular honeycomb lattice, the oscillations have been detected at temperatures between 50 mK and 6 K and below $H \approx 12\,\mathrm{Oe}$. As in the previous experiment, the oscillations were found on a background of positive magneto-resistance indicating the importance of so-called *anti-localization* induced by spin-orbit scattering in these samples.

1.3.2.3 Single mesoscopic rings

Intuitively, one would expect to observe also oscillations with periodicity Φ_0 in samples with geometries such that the electron paths can intersect. These are related to electron states that do not correspond to closed paths but to intersecting non-closed trajectories. In a single ring connected to two wires 1 and 2, such that there are two possibilities for a particle to travel from 1 to 2, the phase difference between the two possible paths is

$$\Delta\varphi(B) = \frac{2\pi e}{h} \oint \boldsymbol{A} \cdot \mathrm{d}\boldsymbol{s} = 2\pi \frac{\Phi}{\Phi_0}. \tag{18}$$

However, as the detailed theory shows, there are random phase factors which are associated with each of these contributions, due to the presence of impurity scattering. In the above experiments the geometries are such that many such terms contribute and have to be summed. The random phase factors add up to zero in this case. In order to verify the existence of the states leading to the periodicity of exactly one flux quantum, a measurement on a single ring has to be undertaken. This has been successfully performed in 1985 [85C, 85D, 85W, 86U] (see also Section 10 for experimental results on semiconductor rings) and constitutes additional experimental evidence for the presence of quantum coherence in normal-metallic, disordered samples at sufficiently low temperature.

1.3.3 Conductance fluctuations

Unexpected reproducible but random fluctuations have been found in the conductance of various mesoscopic samples as a function of parameters such as the density of the charge carriers or an external magnetic field. The conductance is not self-averaging and the fluctuations do not vanish with increasing sample size. Such reproducible conductance fluctuations are a signature of the

randomness of the transport processes combined with quantum coherence. For reviews on this field, not only semiconductor-based systems, see [91A1].

1.3.3.1 Quasi-one dimensional inversion layers in MOSFETs

The first observation was made on metal-oxide-silicon field-effect transistor (MOSFET) accumulation layer samples in which it was possible by a suitable arrangement of doping regions and gates to form quasi-1D conduction channels [82F]. The conductance was found to oscillate randomly but reproducibly as a function of the voltage at the Al-gate (see for example Fig. 121 in Section 7.2.1). The amplitude of the fluctuations has been found to increase with decreasing temperature.

1.3.3.2 Universal magneto-conductance fluctuations

Reproducible fluctuations of the magneto-conductance have also been found to exist in metallic wires with geometrical diameters and lengths smaller than or comparable with the phase coherence length [84U, 85L2, 86K, 86S]. At low temperatures, the amplitude of these fluctuations are of the order of [87L]

$$\Delta G = \frac{e^2}{h}\,, \tag{19}$$

almost independent of the sample properties. Therefore, the fluctuations are called *universal*. For higher temperatures, when the phase coherence length is smaller than the length of a wire, the conductance fluctuations decrease as the square root of the number of the the phase coherent regions $\sqrt{L_\phi(T)/L}$ in the sample, due to the stochastic averaging of the random fluctuations from each region. This is the reason why at high temperatures, the reproducible conductance fluctuations cannot be observed.

The universal conductance fluctuations are completely reproducible for a given sample. When the sample is heated up to room temperature and cooled down again to the measuring temperature, the pattern of the fluctuations is in general changed. This is due to thermally induced microscopic changes of the impurity configuration. Indeed the pattern of the fluctuations is characteristic for the microscopic configuration of the impurities, and the fluctuations are therefore called "magneto-fingerprints".

Together with the periodic and the random fluctuations of the conductance at low temperatures, one observes also nonlocal properties of the electrical transport within length scales of the order of the phase coherent length [87U]. These reflect the quantum mechanical phase coherence over distances of the order of the phase coherence length of the states that participate in the transport processes.

1.3.3.3 Telegraph noise

So far only static fluctuations have been considered resulting from the change of external parameters such as an applied magnetic field or the voltage at a gate or the temperature.

In addition to these, time-dependent switching processes have been observed [87B]. The resistance of Bi-wires with diameters of about 46 nm and lengths of about 60 μm has been measured as a function of the temperature in the region between 50 mK and 5 K. Above 0.8 K the magnitude of the fluctuations has been found to be approximately constant, and of the order of the noise in the measuring circuit. At lower temperatures, the magnitude of the fluctuations was found to be much larger and consistent with the universal conductance fluctuations. When measured as a function of time over a period of a few hours, it turned out that, apart from the measuring system noise, the resistance was constant over long periods but showed sudden jumps at time intervals of the order of 1000 s. The magnitude of these changes were roughly 15 Ω and they were assigned to occasional changes in the microscopic configuration of the impurities involving as few as only one single atom (see Section 11 for more details in semiconducting wires).

1.3.4 The quantum Hall effect

Quantization phenomena of the conductance have been found to be particularly important in semiconductor-based mesoscopic samples. They are of various origins; magnetic and geometrical confinement as well as interaction effects. In the following the historical development is given starting with magnetic confinement effects.

1.3.4.1 Integer quantum Hall effect

The integer quantum Hall effect was discovered in 1980 by Klaus von Klitzing when investigating the transport properties of MOSFETs at high magnetic fields and low temperatures. The magnetoresistance was determined by measuring the voltage $U_{\rm pp}$ between two different probes positioned on the same side of the device between source and drain of the transistor. The Hall resistance was determined by measuring the Hall voltage $U_{\rm H}$ between probes on opposite sides (Fig. 5).

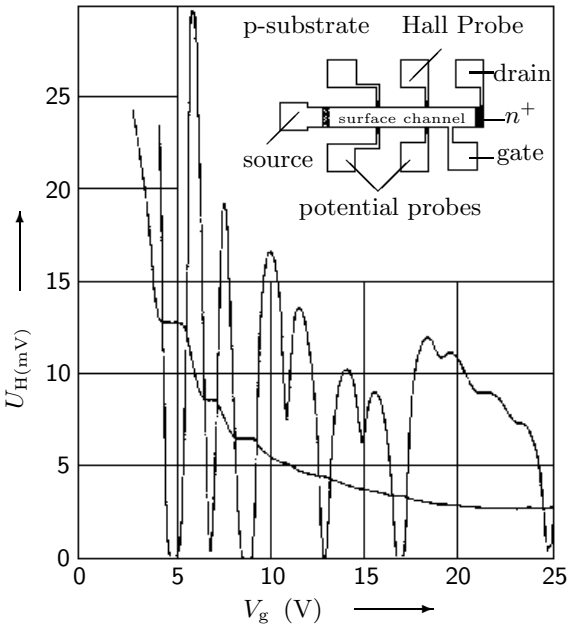

Fig. 5: The Hall voltage $U_{\rm H}$ and the voltage drop between potential probes, $U_{\rm pp}$ as a function of the gate voltage $V_{\rm g}$, at $T = 1.5\,{\rm K}$ and constant magnetic field $B = 18\,{\rm T}$. The source-drain current I has been fixed to 1μ A. Inset: top view of the device; length $L = 400\,\mu{\rm m}$, width $W = 50\,\mu{\rm m}$, distance between potential probes $L_{\rm pp} = 130\,\mu{\rm m}$. Labels at abscissa denote scale for $U_{\rm H}$ in meV, scale for $U_{\rm pp}$ is 1/10 of scale of $U_{\rm H}$ [80K].

The striking and unexpected experimental result was that in certain regions of the gate voltage $V_{\rm g}$, the Hall voltage, instead of varying monotonically as a function of $V_{\rm g}$, remained constant, for fixed source-drain current I. The gate voltage is roughly proportional to the electron density—the Fermi energy—in the inversion layer of a MOSFET. The ratio between the Hall voltage and the source-drain current is the Hall resistance. Thus, the experimental finding implies that the Hall resistance as a function of the Fermi energy exhibits plateaux. The values of the plateaux resistances are found to be independent of the geometry and the internal properties of the sample,

$$R_{\rm H}(i) = \frac{1}{i}\frac{h}{e^2} \equiv \frac{R_{\rm K}}{i}\,, \qquad (i = 1, 2, 3\ldots), \tag{20}$$

with the von Klitzing constant $R_{\rm K} = 25812.8085 \pm 0.0017\Omega$. As the fine structure constant is

$$\alpha = \mu_0 c \frac{e^2}{h} \tag{21}$$

the measurement of the plateau values of the Hall resistance is a measurement of the fine structure constant, since μ_0, the permeability of the vacuum, is exact and c, the speed of light in vacuum, is very precisely known. In the first experiments, the relative inaccuracy of the plateau values was approximately 10^{-5} and limited only by the available voltmeter. Later, by using precision

experimental techniques, the inaccuracy was reduced by several orders of magnitude [82P, 86vK]. Indeed, the reproducibility of the plateaux has been found to be better than that of conventional resistance standards, namely of the order of and better than 10^{-9}. Therefore, the integer quantum Hall effect is nowadays used as a international standard for the unit of the electrical resistance [89T, 91B].

In the regions of the plateaux in the Hall resistance, the voltage $U_{\rm pp}$ has been found to be so small that the corresponding resistance could not be measured with the experimental setup used. Between the plateaux, the longitudinal resistance

$$R = \frac{U_{\rm pp}}{I} \tag{22}$$

shows peaks with widths that depend—as do the widths of the Hall plateaux—in a characteristic way on the temperature.

Theoretically, the integer quantum Hall effect is not fully understood, although it has been the subject of considerable international effort during the past two decades, especially after being rewarded with the Nobel prize in 1985. It is now widely believed, on the basis of field theoretical [83L2] and numerical [95H] evidence that the random potential of the impurities in the MOSFET induce localization in such a way that the localization length as a function of the energy, $\xi(E)$, of the electron states in the inversion layer has singularities near the centres of the disorder broadened Landau bands [93K, 97D]

$$\xi(E) = \frac{\xi_i}{|E - E_i|^s} \,. \tag{23}$$

Here, E_i are energies near the Landau band centres, ξ_i constants and $s = 2.34 \pm 0.04$ a universal critical exponent. At non-zero temperatures, the inversion layer becomes conducting only close to the energies E_i, while it is electrically insulating in the regions of the plateaux. In this way the integer quantum Hall effect is interpreted as a manifestation of a disorder induced metal-insulator transition with critical points near the Landau band centres.

A second approach starts from the edge states which are well known to be present in an electron system in a strong magnetic field [31T, 82H]. In these states, back-scattering is strongly suppressed, and the coherence length can be extremely large, of the order of hundreds of μm. They can be used to explain the plateau values of the Hall resistance [88B].

1.3.4.2 The fractional quantum Hall effect

As a direct consequence of the discovery of the integer quantum Hall effect, similar experiments have been performed also on other semiconductor systems which contain inversion layers of charge carriers, mainly AlGaAs/GaAs heterostructures. In contrast to Si-MOSFETs, these can be fabricated with very few impurities, such that the electron mobility is very high, recently up to a few million $\rm cm^2/Vs$. Then, localization induced by impurities is considerably reduced, and as a consequence, the widths of the Hall plateaux become smaller.

In 1982, researchers at AT&T Bell laboratories discovered additional plateaux of the Hall resistivity in high-mobility AlGaAs/GaAs heterostructures [82T]. The samples had electron mobilities between 80000 and 100000 $\rm cm^2/Vs$. The Hall resistance and the longitudinal resistance were determined as functions of the magnetic field for fixed electron density ($n \approx 10^{11}\,\rm cm^{-2}$) (Figs. 6 and 7). The measurements were performed at temperatures below 4.2 K. Except for the plateaux at integer filling factors

$$\nu = \frac{nh}{eB} \equiv i \tag{24}$$

$\rho_{\rm H}$ was found to exhibit a plateau for $\nu = 1/3$ equivalent to a magnetic field of about 150 kG. Correspondingly, the longitudinal resistivity ρ_{xx} showed a dip near this filling factor [82T].

Later additional experiments revealed a considerable number of plateaux at fractional filling factors [99S]. It has been quickly recognized that an explanation of this "fractional quantum Hall

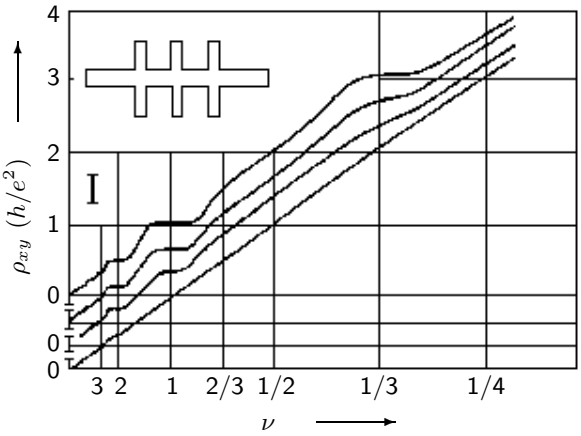

Fig. 6: Hall resistivity ρ_{xy} in units of h/e^2 of a GaAs/$Al_{0.3}Ga_{0.7}$As sample with $n = 1.23 \times 10^{11}\,\mathrm{cm}^{-2}$, mobility $\mu = 90000\,\mathrm{cm}^2/\mathrm{Vs}$ as a function of the filling factor ν which is inverely proportional to the magnetic flux density B, with $I = 1\,\mu\mathrm{A}$.

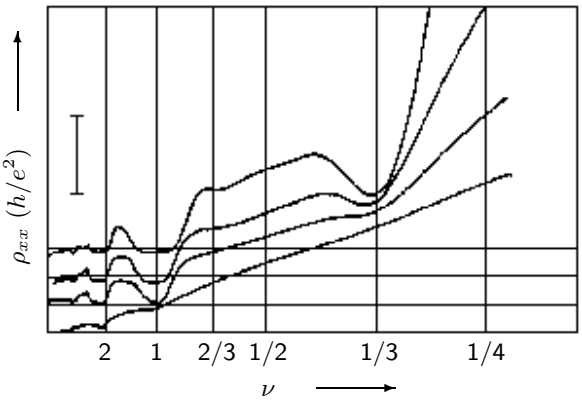

Fig. 7: Longitudinal resistivity ρ_{xx} in units of h/e^2 of a GaAs/$Al_{0.3}Ga_{0.7}$As sample with $n = 1.23 \times 10^{11}\,\mathrm{cm}^{-2}$, mobility $\mu = 90000\,\mathrm{cm}^2/\mathrm{Vs}$ as a function of the filling factor ν which is inverely proportional to the magnetic flux density B, with $I = 1\,\mu\mathrm{A}$.

effect" required the consideration of interactions between the electrons. However, none of the existing many-body theories seemed to be suited to explain the effect. Despite many successes [83L1, 83Y, 89J], there are considerable efforts to find a description for the correlated electron states that are responsible for this striking many-body phenomenon [95M].

It is now common belief that in order to show a plateau in the Hall conductivity, the ground state of the many-electron system should be separated from the energetically lowest excited state by an energy gap. The model of the "incompressible electron fluid" [83L1] introduced on the basis of numerical evidence for a few interacting electrons in a high magnetic field seems to fulfill this requirement for certain rational filling factors with *odd* denominators. "Fundamental fractional states" occur at fillings $1/q$ with $q = 3, 5, 7, \ldots$. In addition, the model predicts quasi-particle excitations that carry fractional charges e^* given by the filling factor, such that $e^* = \pm e/q$ depending on whether the excitations are quasi-electrons or quasi-holes.

Fractional states at filling factors p/q are obtained in this model by starting from the quasi-particles at a fundamental filling and constructing from them a new generation of fractional states. This procedure can be repeated and leads to a hierarchy of many-particle states which contains the experimentally detected fractions as a subset [83Y].

Recently, the concept of the "fractionally charged" quasi-particle excitations has obtained experimental support by direct observation of the fractional charge in noise experiments [97P, 97S].

1.3.5 Resistance quantization in mesoscopic point contacts

In short quantum wires fabricated by using inversion layers in semiconductor heterostructures conductance quantization in units of e^2/h can be observed at low temperatures even without applying a magnetic field (for details see Part II below) [88W, 88vW]. The inversion layer used had a very large electron mobility, the elastic mean free path was of the order of $10\,\mu$m. By applying a negative voltage to a split gate on top of the layered structure, the electron density was depleted underneath the gate except for the small opening of a length of the order of $1\,\mu$m where the width of the electron gas was reduced to less than about $0.5\,\mu$m, depending on the gate

voltage. Without magnetic field, the conductance of such a point contact has been found to be

$$G(E_F) = 2i(E_F)\frac{e^2}{h} \tag{25}$$

where $i(E_F) = 1, 2, 3, \ldots$ is the number of occupied subbands. The factor of 2 results from the spin degeneracy.

By applying a magnetic field, the spin degeneracy of the sub-bands is lifted. As a consequence, between the conductance steps additional plateaux at odd multiples of e^2/h occur (see Section 3.1.6).

This conductance quantization is related to the quantization of the energy as a result of the geometrical constriction of the electrons to the finite cross-section of the wire or point contact. The basic idea can be easily understood by using the following heuristic argument. Due to the constriction, the electron energies corresponding to the transversal modes are quantized, E_j, $j = 1, 2, 3, \ldots$. Only in the longitudinal direction can the electrons move freely, such that the total energy can be written as

$$E_j(k) = E_j + \frac{\hbar^2 k^2}{2m} \tag{26}$$

with m the effective mass and k the wave number corresponding to the x-direction. The Fermi velocity of the jth band is

$$v_j = \sqrt{2(E_F - E_j)/m} \tag{27}$$

and the time needed to travel through the constriction is

$$\tau = \frac{L}{v_j}\,. \tag{28}$$

Inserting this into the Drude formula for the conductivity

$$\sigma = \frac{ne^2\tau}{m} \tag{29}$$

and using the 1D-electron density in the jth sub-band

$$n = \frac{2\sqrt{2m(E_F - E_j)}}{h} \tag{30}$$

yields, after summation of the contributions of $i(E_F)$ subbands

$$\sigma = \frac{2e^2}{h} i(E_F) L \tag{31}$$

which gives the required result (25) for the conductance $G = \sigma/L$.

The quantization is thus seen to result from a compensation between the Fermi velocity and the density of states in 1D. It is obvious that a more complete theory has to take into account impurity scattering and the shape of the constriction, as well as electron-electron interaction, in order to explain why the plateaux occur [88G, 97D].

1.3.6 Conductance oscillations in quantum dots

With two split gates in series, one can control the transport of electrons one by one. This has been demonstrated by using suitable arrangements of tunnel junctions between metal wires [89F] as well as using split gates on semiconductor heterostructures [90M]. Here, only the latter are considered.

Two split gates in series have been fabricated on top of a AlGaAs/GaAs-heterostructure (Fig. 8), and an additional backgate on the rear of the sample, in order to control the electron density

independently of the point contacts formed by the voltage at the split gates. For sufficiently large negative voltage applied to the split gates, an electron island is formed between the two point contacts which is only weakly connected to the outside 2D electron layer by potential barriers. The conductance through this electron island, when measured at mK-temperatures as a function of the voltage applied to the back-gate, exhibits resonance-like peaks which are at periodic in gate voltage (Fig. 9). With decreasing distance between the point contacts, the distance between the peaks is found to increase. The peaks are thermally broadened, but when T is lowered, the broadening does not vanish but saturates at the natural linewidth Γ.

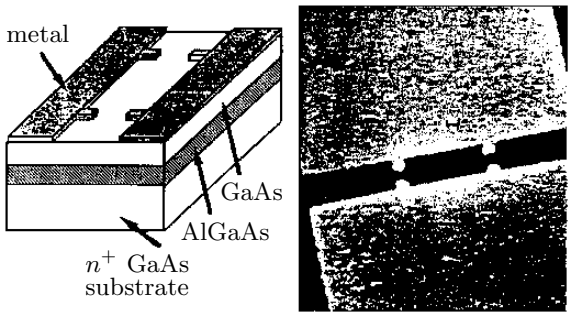

Fig. 8: Left: scheme of a device for measuring Coulomb blockade oscillations of the conductance through an electron island. The 2D electron gas is formed near the interface between the GaAs and the AlGaAs layers. The metal electrodes on top of the structure can be used to define a narrow channel with two potential barriers. Right: scanning electron micrograph of the structure [90M].

The geometry of the electron island, which can be deduced from the experimental setup, is such that the one-electron energy levels are much smaller than the distance between the resonances. Therefore, the effect cannot be simply interpreted as resonant tunnelling through the energy levels of the island. Instead, as a careful analysis of the experimental data shows, the resonances are due to the Coulomb blockade effect [89F]. Each resonance corresponds to the sequential transport of single electrons through the island. This can be understood by using a simple classical argument.

Electrons can move in and out from the island if their chemical potential is identical to that of the surrounding inversion layer. The former is the difference between the energies of the ground states of N and $N+1$ electrons, the latter is E_{F}. The condition for transport is thus

$$E_{\mathrm{F}} = E(N+1) - E(N) \tag{32}$$

The ground state energy $E(N)$ is, neglecting the single particle spectrum, approximately the electrostatic energy of N electrons on the island, given by

$$E(N) \approx \frac{e^2 N^2}{2C}, \tag{33}$$

with C the capacitance of the island. This implies that transport is possible if

$$E_{\mathrm{F}}(N) = \frac{Ne^2}{C} \propto e(V_{\mathrm{g}} - V_{\mathrm{th}}). \tag{34}$$

where V_{th} is a threshold above which the oscillations appear. Since in the experiment the peaks are equidistant, the capacitance is independent of the electron number, and may be quantitatively determined.

Coulomb blockade oscillations have also been observed at room temperature [92S]. The effect may be used to construct a current standard by frequency-controlling the number of electrons passing the device [90G]. Also, single electron transistors may be constructed [91A2, 97D].

In addition, the blockade effect may be used to investigate the N-particle excitation spectra of the interacting electrons by nonlinear transport experiments [92J, 93W, 95W].

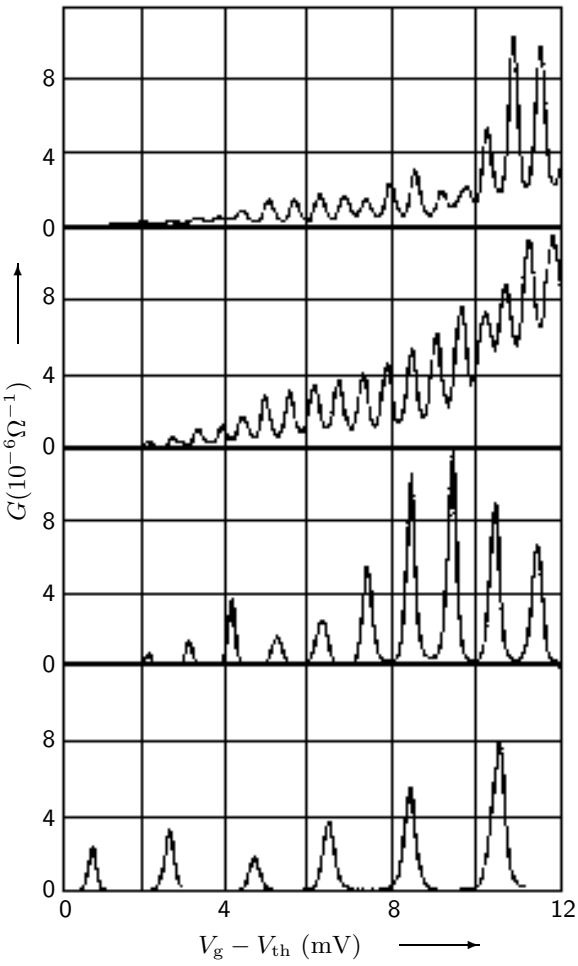

Fig. 9: Conductance at $T = 50\,\mathrm{mK}$ as a function of the voltage V_g applied to the back-gate of the structure shown in Fig. 8, relative to a threshold voltage V_t. [90M]; uppermost top and next top: results for samples with the same geometry of the gates; upermost bottom and lowest: results for progressively smaller distance between the two constrictions, with corresponding increase of the period of the oscillations.

1.3.7 Persistent currents in non-superconducting rings

A further important example of a mesoscopic quantum effect is the persistent current in a normally conducting metallic ring which is pierced by an Aharonov-Bohm flux. This is not a non-equilibrium transport phenomenon, but an *equilibrium property* of the electronic ground state in the presence of the flux. This effect was predicted already in the early days of quantum mechanics [38H] and has been re-discussed later in the context of mesoscopic transport [85B].

An elementary approach for the understanding of the phenomenon is to consider a 1D wire of the length L with generalized periodic boundary conditions for the wave function

$$\psi(x) = e^{i\varphi}\psi(x+L)\,. \tag{35}$$

This leads to eigen-energies

$$\varepsilon(\varphi) = \frac{\hbar^2 k^2}{2m} \tag{36}$$

with allowed wave numbers

$$k = \frac{2\pi}{L}\left(n - \frac{\varphi}{2\pi}\right)\,. \tag{37}$$

Introducing now an Aharonov-Bohm flux Φ piercing the ring it turns out that the eigen-energies are again given by the above (36) but with the replacement $\varphi \to 2\pi\Phi/\Phi_0$. The spectrum is periodic with the period 1. The persistent current can be obtained from the total energy of the electrons in the ground state by

$$I(\Phi) = -\frac{\mathrm{d}E(\Phi)}{\mathrm{d}\Phi} \tag{38}$$

which corresponds to a magnetisation

$$M(\Phi) = -\frac{\mathrm{d}E}{\mathrm{d}B} = -\frac{L^2}{4\pi}\frac{\mathrm{d}E}{\mathrm{d}\Phi}\,. \tag{39}$$

Despite the early theoretical work the first experimental observation of a persistent current has been achieved only recently [90L]. The experiment was performed on a Cu grid consisting of about 10^7 squares Cu-rings with a sidelength of $0.55\,\mu$m and did not become superconducting. The rings were fabricated by using electron beam lithography, and the experiments were performed at temperatures between 7 mK and 200 mK. The magnetisation of the rings was measured with a calibrated ultra-sensitive SQUID magnetometer using a differential technique.

Although the mean free path of the electrons in the rings was only a few nm, it was possible to detect the persistent current via the corresponding magnetic moment. The effect has been found to be an order of magnitude larger than predicted by the theory [91I]. This is still not fully understood, and remains a challenge to the theory.

The experiment has been repeated several times using single Au-rings [91C] and single electron rings made by using semiconductor inversion layers in an AlGaAs/GaAs heterostructure [93M]. Only the results of the latter experiment have been found to be consistent with the theoretically predicted order of magnitude of the persistent current.

1.4 References for Section 1

[30L] Landau, L.: Z. Phys. **64** (1930) 629.

[31T] Teller, E.: Z. Phys. **67** (1931) 311.

[33P] Peierls, R.: Z. Phys. **80** (1933) 763.

[38H] Hund, F.: Ann. der Phys. 5. Folge **32** (1938) 102.

[50M] MacDonald, D.K.C., Mendelson, K.: Proc. Roy. Soc. (London) A**202** (1950) 103.

[66L] Langer. J.S., Neal, T.: Phys. Rev. Lett. **16** (1966) 984.

[72Z] Ziman, J.M.: Electrons and Phonons (Clarendon Press, Oxford 1972).

[74T] Thouless, D.J.: Phys. Rep. **13** (1974) 93.

[76A] Ashcroft, N.W., Mermin, N.D.: Solid State Physics (Holt, Winehart and Winston, 1976).

[79A] Abrahams, E., Anderson, P.W., Licciardello, D.C., Ramakrishnan, T.V.: Phys. Rev. Lett. **42** (1979) 673.

[79D] Dolan, G.J., Osheroff, D.D.: Phys. Rev. Lett. **43** (1979) 196.

[79G] Gor'kov, L.P., Larkin, A.I., Khmel'nitskii, D.E.: JETP Lett. **30** (1979) 228.

[80K] von Klitzing, K., Dorda, G., Pepper, M.: Phys. Rev. Lett. **45** (1980) 494.

[81A] Altshuler, B. L., Aharonov, A. G., Spivak, B. Z.: JETP Lett. **33** (1981) 94.

[81S] Sharvin, D. Yu., Sharvin, Yu. V.: JETP Lett. **34** (1981) 272.

[81V] Van den Dries, L., Van Haesendonck, C., Bruynseraede, Y., Deutscher, G.: Phys. Rev. Lett. **46** (1991) 565.

[82F] Fowler, A.B., Hartstein, A., Webb, R.A.: Phys. Rev. Lett. **48** (1982) 196.

[82H] Halperin, B.I.: Phys. Rev. B**25** (1982) 2185.

[82P] Paalanen, M.A., Tsui, D.C., Gossard, A.C.: Phys. Rev. B**25** (1982) 5566.

[82T] Tsui, D.C., Störmer, H.L., Gossard, A.C.: Phys. Rev. Lett. **48** (1982) 1559.

[83L1] Laughlin, R.B.: Phys. Rev. Lett. **50** (1983) 1395.

[83L2] Levine, H., Libby, S.B., Pruisken, A.M.M.: Phys. Rev. Lett. **51** (1983) 1915.

[83Y] Yoshioka, D., Halperin B.I.: Phys. Rev. Lett. **50** (1983) 1219.

[84A] Aronov, A.G., Altshuler, B.L., in: Electron-Electron Interactions in Disordered Solids, M. Pollak, A.L. Efros (Eds.) (North-Holland, Amsterdam 1984) p. 1.

[84B] Bergmann, G.: Phys. Rev. **107** (1984) 1.

[84F] Fukuyama, H., in: Electron-Electron Interactions in Disordered Solids, M. Pollak, A. L. Efros (Eds.) (North-Holland, Amsterdam 1984) p. 155.

[84L] Laughlin, R.B.: Surf. Sci. **142** (1984) 163.

[84P] Pannetier, B., Chaussy, J., Rammal, R., Gandit, P.: Phys. Rev. Lett. **53** (1984) 718.

[84U] Umbach, C. P., Washburn, S., Laibowitz, R. B., Webb, R. A.: Phys. Rev. B**30** (1984) 4048.

[85B] Büttiker, M., Imry, Y., Landauer, R.: Phys. Lett. A**96** (1985) 365.

[85C] Chandrasekar, V., Rooks, M. J., Wind, S., Prober, D. E.: Phys. Rev. Lett. **55** (1985) 1610.

[85D] Datta, S., Melloch, M. R., Bandyopadhyay, S., Noren. R., Vaziri, M., Miller, M., Reifenberger, R.: Phys. Rev. Lett. **55** (1985) 2344.

[85L1] Lee, P.A., Ramakrishnan, T.V.: Rev. Mod. Phys. **57** (1985) 287.

[85L2] Licini, J.C., Bishop, D.J., Kastner, M.A., Melngailis, J.: Phys. Rev. Lett. **55** (1985) 2987.

[85W] Webb, R. A., Washburn, S., Umbach, C.P., Laibowitz, R.B.: Phys. Rev. Lett. **54** (1985) 2696.

[86K] Kaplan, S.B., Hartstein, A.: Phys. Rev. Lett. **56** (1986) 2403.

[86vK] von Klitzing, K.: Rev. Mod. Phys. **58** (1986) 519.

[86S] Skocpol, W.J., Mankiewich, P.M., Howard, R.E., Jackel, L.D., Tennant, D.M., Stone, A.D.: Phys. Rev. Lett. **56** (1986) 2865.

[86U] Umbach, C. P., Van Haesendonck, C., Laibowitz, R.B., Washburn, S., Webb, R.A.: Phys. Rev. Lett. **56** (1986) 386.

[87A] Aharonov, A.G., Sharvin, Yu.V.: Rev. Mod. Phys. **59** (1987) 755.
[87B] Beutler, D.E., Meisenheimer, T.L., Giordano, N.: Phys. Rev. Lett. **58** (1987) 1240.
[87L] Lee, P.A., Stone, A.D., Fukuyama, H.: Phys. Rev. B**35** (1987) 1039.
[87U] Umbach, C.P., Santhanam, P., Van Haesendonck, C., Webb, R.A.: Appl. Phys. Lett. **50** (1987) 1289.
[88B] Büttiker, M.: Phys. Rev. B**38** (1988) 9376.
[88G] Glazman, L.I., Lesovik, G.B., Khmel'nitskii, D.E., Shekter, R.I.: JETP Lett. **48** (1988) 239.
[88vW] van Wees, B.J., van Houten, H., Beenakker, C.W.J., Williamson, J.G., Kouwenhoven, L.P., van der Marel, D., Foxon, C.T.: Phys. Rev. Lett. **60** (1988) 84.
[88W] Wharam D.A., Thorton, T.J., Newbury, R., Pepper, M., Ahmed, H., Frost, J.E.F., Hasko, D.G., Peacock, D.C., Ritchie, D.A., Jones, G.A.C.: J. Phys. C: Solid State Phys. **21** (1988) L209.
[89J] Jain, J.K.: Phys. Rev. Lett. **63** (1989) 199.
[89F] Fulton, T.A., Gammel, P.L., Bishop, D.J., Dunkleberger, L.N., Dolan, G.J.: Phys. Rev. Lett. **63** (1990) 1307.
[89T] Taylor, B N., Witt, T.J.: Metrologia **26** (1989) 47.
[90G] Geerligs, L.J., Anderegg, V.F., Holweg, P.A.M., Mooij, J.E., Pothier, H., Esteve, D., Urbina, C., Devoret, M.H.: Phys. Rev. Lett. **64** (1990) 2691.
[90L] Levy, L. P., Dolan, G., Dunsmuir, J., Bouchiat, H.: Phys. Rev. Lett. **64** (1990) 2074.
[90M] Meirav, U., Kastner, M.A., Wind, S.: Phys. Rev. Lett. **65** (1990) 771.
[91A1] Althuler, B.L., Lee, P.A., Webb, R.A. (Eds.): Mesoscopic Phenomena in Solids. (North-Holland, Amsterdam 1991).
[91A2] Averin, D.V., Likharev, K.K.: in: Mesoscopic Phenomena in Solids, B.L. Altshuler, P.A. Lee, R.A. Webb (Eds.) (North-Holland, Amsterdam 1991) p. 273.
[91B] Braun, E.: in Units and Fundamental Constants in Physics and Chemistry. J. Bortfeldt, B. Kramer (Eds.), Landolt-Börnstein, New Series (Springer Verlag, Berlin 1991) p. 2.
[91C] Chandrasekhar, V., Webb, R.A., Brady, M.J., Ketchen, M.B., Gallagher, W.J., Kleinsasser, A.: Phys. Rev. Lett. **67** (1991) 3587.
[91I] Imry, Y.: in: Quantum Coherence in Mesoscopic Systems, B. Kramer (Ed.), NATO ASI Ser. B **254** (Plenum Press, New York 1991) p. 221.
[92J] Johnson, A.T., Kouwenhoven, L.P., de Jong, W., van der Vaart, N.C., Harmans, C.J.P.M.: Phys. Rev. Lett. **69** (1992) 1592.
[92S] Schönenberger, C., van Houten, H., Donkersloot, H.C.: Europhys. Lett. **20** (1992) 249.
[92V] Vollhardt, D., Wölfle, P.: in: Electronic Phase Transitions, W. Hanke, Y.V. Kopaev, (Eds.) (North-Holland, Amsterdam 1992) p. 1.
[93K] Kramer, B., MacKinnon, A.: Rep. Progr. Phys. **56** (1993) 1549.
[93M] Mailly, D., Chapelier, C., Benoit, A.: Phys. Rev. Lett. **70** (1993) 2020.
[93W] Weis, J., Haug, R.J., von Klitzing, K., Ploog, K.: Phys. Rev. Lett. **71** (1993) 4019.
[95H] Huckestein, B.: Rev. Mod. Phys. **67** (1995) 357.
[95M] MacDonald, A.H.: in: Quantum Transport in Semiconductor Submicron Structures., B. Kramer (Ed.) (Kluwer, Dordrecht 1995) p. 63.
[95W] Weinmann, D., Häusler, W., Kramer, B.: Phys. Rev. Lett. **64** (1995) 984.
[97D] Dittrich T., Hänggi, P., Ingold, G.-L., Kramer, B., Schön, G., Zwerger, W.: Quantum Transport and Dissipation. (Wiley-VCH, Weinheim 1997) p. 79.
[97M] Mohanty, P., Jariwala, E.M.Q., Webb, R.A.: Phys. Rev. Lett. **78** (1997) 3366.
[97P] de Picciotto, R., Reznikov, M., Heiblum, M., Umansky, V., Bunin, G., Mahalu, D.: Nature **389** (1997) 162.
[97S] Saminadayar, L., Glättli, D.C., Etienne, B.: Phys. Rev. Lett. **79** (1997) 2526.
[99S] Störmer, H.L.: Rev. Mod. Phys. **71** (1999) 875.